Electrochimica Acta 285 (2018) 60–69

Contents lists available at ScienceDirect

Electrochimica Acta

journal homepage: www.elsevier.com/locate/electacta

Synthesis of uniform bulk nanoporous palladium with tunable structure

Shan Shi [a, *], Jürgen Markmann [a, b], Jörg Weissmüller [b, a]

[a] Institute of Materials Research, Materials Mechanics, Helmholtz-Zentrum Geesthacht, Germany
[b] Institute of Materials Physics and Technology, Hamburg University of Technology, Germany

ARTICLE INFO

Article history:
Received 5 May 2018
Received in revised form
9 July 2018
Accepted 14 July 2018
Available online 20 July 2018

Keywords:
Nanoporous palladium
Dealloying
Coarsening

ABSTRACT

This work presents systematic investigations on the synthesis of hierarchical nanoporous Pd via electrochemical dealloying of CuPd alloys in sulfuric acid. The impact of electrode potential, dealloying temperature, and additional annealing on microstructure and morphology is explored. Dealloying $Cu_{85}Pd_{15}$ in 1M sulfuric acid at elevated temperature provides a facile strategy to produce bulk nanoporous Pd samples which are uniform, hierarchically nanoporous, and free of macro-scale cracks. The question "Why will one-step template-free dealloying yield a hierarchical and not unimodal nanoporous structure?" is discussed. The impact of passivation and of a percolating Cu-rich cluster on the pore structure is inspected. A structural instability concept for dealloying of dilute master alloys is preferred as the underlying mechanism. Nanoporous Pd with classical, unimodal pore structure and tunable ligament size ranging from 80 to 270 nm emerges when the as-prepared hierarchical nanoporous Pd is annealed. The material of this study may provide a model system that complements nanoporous Au for studies of bulk nanoscale metal networks as functional and structural materials.

1. Introduction

Dealloying involves the selective dissolution of the less noble component from a solid solution or compound via free or electrochemical corrosion. The more noble component diffuses and aggregates into an open cell nanoporous structure in three dimensions [1,2]. Monolithic bodies of nanoporous metal are distinguished by their large surface area, tunable structure size and good mechanical behavior. This predestines them as materials with novel functionality [3], specifically in catalysis [4–6], actuation [7–12], sensing [13–18], and energy storage [19]. Besides function, the mechanical behavior of nanoporous metal is of significant current interest. While early reports on the extremely high local strength of the ligaments of nanoporous metal rested on small-scale testing techniques [20,21], the advent of preparation protocols for macroscopic nanoporous metal bodies with high deformability and with excellent homogeneity, reproducibility and structural control led to a shift of focus towards millimeter- or centimeter-sized samples that can be tested with robust macroscale approaches [22–28]. Their quality as exceptionally well-defined model system for studies of small-scale mechanical behavior is exemplified by conventional mechanical tests on bulk nanoporous gold samples, which enable the investigations on how ligament size and surface state influence the macroscopic elastic, plastic and fracture behavior [29–33]. Controlling and understanding mechanical properties of nanoporous (np) metals is also crucial for their performance as functional materials.

In view of the significance of uniform and mechanically resilient macroscopic bodies for studies of nanoporous metals as structural and functional materials it is significant that macroscale studies of mechanics and function of dealloying-made nanoporous metals have so far been largely restricted to nanoporous gold. It would be desirable to extend the materials' base by establishing preparation protocols that yield metals other than gold in the form of macroscopic, uniform and deformable bodies with tunable structure size. One approach in this direction is liquid metal dealloying, which yields porous titanium, niobium, or stainless steel [34–37]. Yet, liquid metal dealloying typically yields ligament sizes well above hundred nanometers, preventing the study of many of the size effects that are of interest to small-scale plasticity. Here, we present an aqueous dealloying approach towards nanoporous Pd with uniform microstructure and with a structure size that can be tuned between few nm and a few hundred nm.

* Corresponding author.
E-mail address: shan.shi@hzg.de (S. Shi).

https://doi.org/10.1016/j.electacta.2018.07.081

Recently, nanoporous metals with hierarchical structure providing large specific surface area for functionalization and wide transport pathway for fast response are of particular interest [10,38–41]. For example, significantly enhanced catalysis properties were realized by using hierarchical nanoporous palladium (np Pd) sheets with pore size of 50 nm and 10 nm [42]. While unimodal np metals typically emerge from dealloying of single-phase solid solutions, the synthesis of hierarchical np metals often uses more complex strategies, such as template-dealloying, dealloying-coarsening-dealloying sequences, and one-step dealloying multiphase alloy or ternary alloy [16,38,40,43,44]. These strategies are well-studied but can be time-consuming or result in inhomogeneous pores at the upper hierarchy level.

In an earlier study, we have reported that one-step dealloying bimetallic $Cu_{85}Pd_{15}$ alloy in 1M sulfuric acid at elevated temperature yields np Pd with a hierarchical pore structure and excellent plastic deformability [11]. The facile protocol produces a uniform pore structure at each hierarchy level, in mm-size samples without cracks. However, the underlying mechanism remains to be understood. In this work, we systematically investigate the underlying electrochemical dealloying steps and we discuss the underlying mechanism of nanostructure formation. We find that annealing the hierarchical np Pd yields unimodal pore structures with ligament size tunable in the range of tens of nm to hundreds of nm. Thus, np Pd made by aqueous dealloying of Cu-Pd may provide np Pd samples that complement np gold as a model system for studying size- and interface effects in nanoporous materials for strength and function.

2. Experimental

2.1. Sample preparation

2.1.1. Master alloy preparation

Ingots of single-phase $Cu_{85}Pd_{15}$, $Cu_{80}Pd_{20}$ and $Cu_{75}Pd_{25}$ alloy were prepared separately by alloying Cu (99.99%, Alfa Aesar) and Pd (99.95%, Heraeus Metals) under argon atmosphere through repeated melting/solidification in an arc melter (MAM-1, Edmund Bühler). The ingot was vacuum-sealed into a quartz glass tube, and then homogenized at 850°C for 5 days followed by quenching in water. Subsequently, it was cold-rolled and cut into cuboids, around $1 \times 1 \times 1 mm^3$ in size by using a diamond wire saw (Model 3032 Horizontal Diamond Wire Saw, Well); no further recovery annealing was imposed [11].

2.1.2. Electrochemical dealloying

Electrochemical dealloying was performed in a three-electrode chemical cell containing 1M H_2SO_4 aqueous electrolyte. The cell was constructed with a double wall enabling a flow of heating/cooling water (Circulating Bath AC200-A28, Fisher Scientific) around the electrolyte making temperature control during electrochemical processes possible. The master alloy cuboids acted as working electrode (WE), coiled Cu wire was used as counter electrode (CE), and a commercial Ag/AgCl/3M KCl electrode (Sigma-Aldrich) as reference electrode (RE). Note that the RE was always calibrated against a standard hydrogen electrode (SHE, HydroFlex, Gaskatel) in the same electrolyte before the dealloying process was initiated. Therefore, all potentials in this work could be and were specified versus SHE. The dealloying process applied a constant electrode potential until the current fell below 10 μA. A potentiostat (PGSTAT302N, Metrohm) was used for all the electrochemical experiments in this work. Afterwards, the as-dealloyed np Pd sample was immersed in ultrapure water (Ultra Clear TWF UV TM, Siemens) for at least 3 h before further electrochemical reduction.

2.1.3. Electrochemical reduction

The electrochemical reduction method is a common strategy used for further removal of less noble metals from dealloying-made nanoporous metals. 10 potential cycles were imposed between 0.2 V and 1.2 V vs. SHE at a scan rate of 10 mV/s on as-dealloyed samples in 1M H_2SO_4 at room temperature. During this treatment, a piece of highly porous carbon cloth (specific surface area 1200–1750 m^2/g, Kynol) was used as CE. Finally, the samples were immersed in ultrapure water for 6 h and ethanol (≥99.5%,Merk) for another 6 h, followed by 24 h drying in argon atmosphere.

2.1.4. Post synthesis thermal annealing

Np Pd Samples synthesized in the way described in the preceding paragraphs were referred to as-prepared samples. In some cases an additional heat treatment was applied. These samples were annealed at the indicated temperature for 5 min in a high-vacuum furnace (MILA-5000, ULVAC) at a pressure below $2 \cdot 10^{-6}$ mbar.

2.2. Characterization

2.2.1. Potentiodynamic polarization

A potentiodynamic polarization approach was used to analyze electrochemical activities of the (massive, not porous) base materials Cu, Pd, and their alloys in various electrolytes. Cu and Pd samples were 2–3 mm long cylinders, cut from Cu (99.99%, Alfa Aesar) and Pd (99.95%, Heraeus Metals) wires of diameter 1 mm. CuPd alloys were cuboids of ~ 1 mm edge length, cut from a rolled alloy sheet. Before characterization, all samples were sequentially treated in an ultrasonic cleaner, using acetone and ethanol for ten minutes each; they were then dried at room temperature.

The polarization curves were measured under a potential scan rate of 1 mV/s, displayed in logarithmic scale of the absolute value of current density against electrode potential. As during synthesis, these measurements were carried out in a three-electrode chemical cell with the same Ag/AgCl/3M KCl electrode as RE. Measuring nonporous bulk metals, we chose a simple piece of 3 cm × 4 cm-sized gold foil to act as CE. Fresh electrolyte was used for every polarization measurement of each material. The geometric area, as determined from the original outer dimensions of the immersed sample, was used to translate electric currents into current densities.

2.2.2. Scanning electron microscopy

The microstructure of np Pd was investigated by scanning electron microscopy (SEM). A FEI Helios NanoLab G3 SEM with immersion lens was used at an accelerating voltage of 2.5 kV and a probe current of 25 pA under 2 mm working distance. Morphologies of fracture surfaces of bulk np Pd samples were analyzed. These cross-sectional surfaces through the sample center were obtained by cutting them with a scalpel. The samples of interest were then glued on standard SEM stubs with the help of silver paint and dried in a fume hood before locking them into the SEM.

2.2.3. X-ray energy-dispersive spectroscopy

Composition analysis was performed on the cross-sections of samples using an energy-dispersive X-ray detector (Oxford X-Max 20 SDD) equipped in the above mentioned SEM. For this type of analysis, an electron beam with an accelerating voltage of 15 kV was focused on the sample with a working distance of around 4 mm. Spectra for spots from edge positions to the central part were measured and analyzed. All given compositions are in atomic percent.

2.2.4. In-situ dilatometry

An in-situ dilatometer setup for the dealloying process was constructed consisting of a potentiostat (PGSTAT302N, Metrohm), a 3-electrode chemical cell, and a vertical dilatometer (Linseis L75V). Typically, a one mm-sized sample of the initial CuPd alloy was placed on top of a thin gold foil and fixed by the dilatometer's pushrod from the top with a constant contact force of 150 mN, corresponding to an effective compressive stress of around 0.15 MPa. The sample clamped by the pushrod was placed close to the Luggin capillary of the 3-electrode chemical cell. In that way, precise dimension changes of the sample during the dealloying process could be recorded.

3. Results

3.1. Electrochemical activities of Cu-Pd alloys

The Cu-Pd binary alloy system was chosen for two reasons: Firstly, Cu and Pd form a continuous series of solid solutions [45], favoring the preparation of homogeneous single-phase master alloys. Secondly, the equilibrium metal/metal ion potential difference between Cu and Pd is more than 0.5 V, suggesting that Cu can be dissolved selectively, leaving metallic Pd. It is accepted that the success of making uniform and homogeneous nanoporous metals by dealloying is related to the balance between dissolution rate of the less noble component and activity of surface diffusion of the remaining noble metal [1,2,46]. This balance can be influenced by several parameters such as the nature of electrolyte, master alloy constituents, and dealloying temperature [47]. Here, we explored specifically the influence of master alloy composition, electrolyte concentration, and dealloying temperature. The master alloy composition $Cu_{75}Pd_{25}$ provides for a comparison with the well-studied dealloying of $Ag_{75}Au_{25}$. Since the dealloying kinetics in $Cu_{75}Pd_{25}$ was found sluggish, $Cu_{85}Pd_{15}$ was included as an alloy with higher less-noble element content and faster corrosion.

Fig. 1a shows polarization plots of pure Cu and Pd in H_2SO_4 aqueous solution with different concentration. It is observed that beyond the corrosion potential, the current density of Cu, which represents the corrosion rate, increases sharply with applied potential. By contrast, Pd shows a much smaller current density than Cu. This indicates that Cu is electrochemically considerably more active than Pd in sulfuric acid. The largest corrosion rate of Cu was observed in 1.0M H_2SO_4. It was also observed that the corrosion potential of Cu was shifted to lower potentials with increasing concentration of sulfuric acid, while Pd showed just the opposite trend. In other words, corrosion potential differences between Cu and Pd enlarge with increasing concentration of sulfuric acid. Their corrosion potential difference rises over 0.5 V in 1.0M H_2SO_4.

Polarization analysis of $Cu_{75}Pd_{25}$ corrosion in differently concentrated H_2SO_4 is displayed in Fig. 1b. $Cu_{75}Pd_{25}$ shows a similar trend as pure Cu in the variation of both corrosion rate and corrosion potential with acid concentration, i.e. as the concentration of H_2SO_4 increases, the corrosion potential decreases and the current densities at specific potentials increase. This further confirms that dissolution of Cu is the easiest and fastest in 1M H_2SO_4 in comparison to the more diluted electrolytes. Therefore, 1M H_2SO_4 was chosen as our electrolyte for the following electrochemical experiments. Yet, even in 1M H_2SO_4 the maximum value of corrosion current density is much less than 1 mA/cm^2. That value is considered as an empirical lower limit for complete dealloying of bulk samples [48,49]; significantly less current density means excessive duration of dealloying. Our further experiments therefore focused on $Cu_{85}Pd_{15}$, which provides for considerably faster corrosion.

Fig. 2 shows polarization plots of $Cu_{75}Pd_{25}$ and $Cu_{85}Pd_{15}$ in 1.0M H_2SO_4, compared with plots from pure Cu and Pd measured at the same conditions as reference. It can be seen that the corrosion behavior of Cu-Pd alloys is somewhat an intermediate between that of pure Cu and pure Pd. But influences from the composition of master alloy on corrosion behavior are apparent. The maximum current density as represented by the corrosion rate increases with

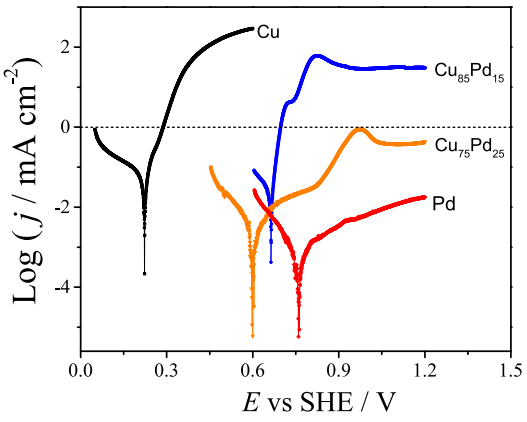

Fig. 2. Polarization plots of Cu, Pd, $Cu_{75}Pd_{25}$, and $Cu_{85}Pd_{15}$ in 1.0M H_2SO_4 at 25°C. The scan rate was 1 mV/s.

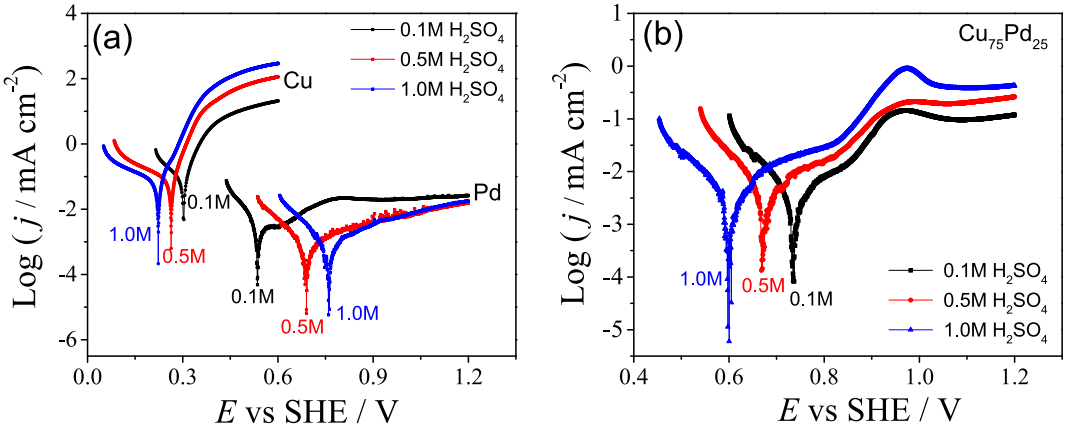

Fig. 1. Polarization plots of (a) pure Cu, Pd and (b) the alloy $Cu_{75}Pd_{25}$ in 0.1M, 0.5M, and 1.0M H_2SO_4 at 25°C. The scan rate was 1 mV/s and *j* denotes the current per original geometric area.

increasing copper content in the master alloy. A current density of more than the critical value of 1 mA/cm^2 is easily obtained in the polarization curve of $Cu_{85}Pd_{15}$ if the applied potential is above 0.7 V vs. SHE.

3.2. Dimension change during dealloying processes

The dealloying potential is crucial for the development of the porous structure and, consequently, for obtaining good structural integrity and mechanical properties in bulk np metals [50–52]. The dimension changes of $Cu_{85}Pd_{15}$ during dealloying in 1M H_2SO_4 at 60°C and different dealloying potentials were explored by in-situ dilatometry. When the dealloying potential was less than 770 mV vs. SHE, the corrosion was slow and even terminated before the material was fully corroded. Dealloying potentials above 820 mV vs. SHE led to fast dealloying and to completely dealloyed samples, yet at the expense of severe cracking and loss of structural integrity. Further detailed studies therefore focused on the intermediate range of dealloying potentials, 778–818 mV.

Fig. 3 shows both the dimension changes and current transients during dealloying in the above mentioned potential range. The relationship between total shrinkage and dealloying potential is summarized in the inset picture in Fig. 3a, indicating that dealloying at a higher potential induces larger shrinkage. The relationship between dealloying duration and electrode potential, see inset in Fig. 3b, shows faster dealloying at higher potential.

On the basis of Faraday's law, the amount of dissolved Cu during the dealloying process can be estimated from the charge accumulated by integration of the measured current in Fig. 3b. This estimation indicates that typically 97±1% of the total amount of Cu in the initial alloy was dissolved into the electrolyte in case of all investigated dealloying potentials in Fig. 3, resulting in a mean residual Cu concentration of about 15 at% Cu in the as-dealloyed state. As described in the sample preparation section, this concentration is further reduced by electrochemical reduction to values of about 5.5 at% varying ±2 at% between different samples, as determined from EDX measurements (no distinct correlation between the investigated dealloying parameters and the residual Cu content was found).

In the above context, it is apposite to present the resulting solid fraction after the complete preparation procedure. Taking into account the dealloying efficiency and dimension shrinkage, 790 mV, at which potential dealloying took about 16 h and caused less than 1% net length shrinkage, was preferred as the dealloying potential for sample preparation in subsequent studies. By application of a simple rule of mixture based on the density of pure Pd and Cu, the theoretical density of a fully dense sample could be determined. The outer dimensions, as measured in an optical microscope, provided the basis for estimating the samples' volume. Volume and mass of the samples imply the solid fraction, that is, the ratio between the densities of the np material and of its solid phase. For the fully dealloyed and electrochemically reduced samples we found as 17%, as already reported in Ref. [11].

3.3. Influence of dealloying temperature on the morphology

The dealloying process involves the balance between dissolution of the less noble component and a trend for passivation due to surface diffusion of the remaining noble metal during dealloying. This balance influences the pore structure and may be used to adjust ligament or pore sizes in common unimodal np materials [1,53,54].

Fig. 4 shows SEM images of fracture surfaces from samples that were prepared by electrochemical dealloying mm-sized $Cu_{85}Pd_{15}$ master alloys in 1M H_2SO_4 at 25°C, 60°C and 80°C. It is seen that a one-step dealloying of this alloy at these three different temperatures yields a uniform but hierarchical nanoporous structure throughout the entire sample. Fig. 4a–b, showing samples dealloyed at 25°C, evidence an ultrafine hierarchical np structure. Fig. 4a shows that the upper level ligament sizes range between 10 nm and 20 nm and the high magnification image in Fig. 4b shows that ultrasmall pores, i.e. less than 5 nm in diameter, exist inside these ligaments.

Fig. 4c–d also show a well-defined two level hierarchy in the np Pd sample obtained with a dealloying temperature of 60°C. By measuring the diameter of randomly chosen ligaments, the mean ligament sizes are found around 35 nm for the upper hierarchical level and below 10 nm for the lower hierarchical level, consistent with our previous observations [11]. Finally, Fig. 4e–f shows the microstructure of a np Pd sample obtained at a dealloying temperature of 80°C. Fig. 4e shows that the mean ligament size of the upper hierarchical level is slightly larger than that obtained at 60°C in Fig. 4c. While Fig. 4f shows that at the lower level, the ligament size obviously is coarser and the total volume of lower-level pores significantly lower in comparison to that obtained at 60°C in Fig. 4d.

3.4. Influence of master alloy composition on the morphology

It is of interest to explore how far the observation of a bimodal

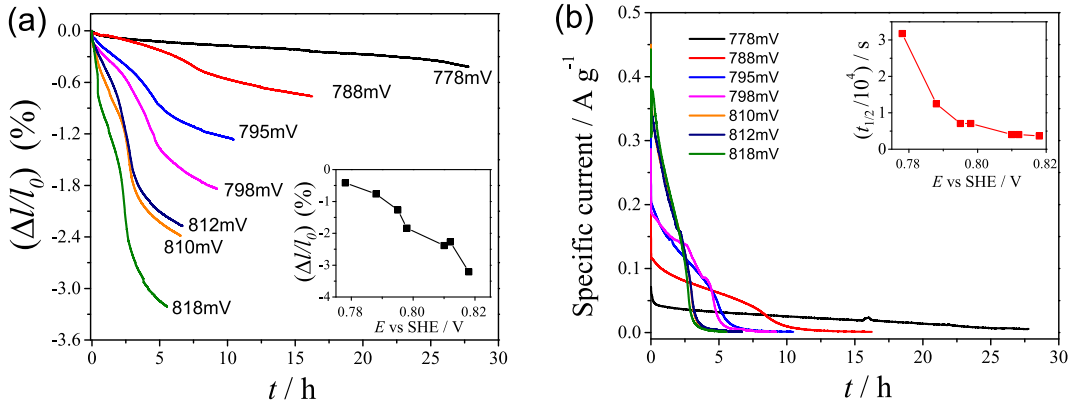

Fig. 3. Influence of the applied potential during dealloying of $Cu_{85}Pd_{15}$ in 1.0M H_2SO_4 at 60°C: (a) Dimension change vs. time during dealloying. The inset picture shows the total shrinkage vs. the dealloying potential. (b) Mass-specific current vs. time during the dealloying process. The inset picture shows the half time, $t_{0.5}$, versus dealloying potential. Here, the half time is defined as the time required to transport half of the charge to the WE as compared to the complete dealloying.

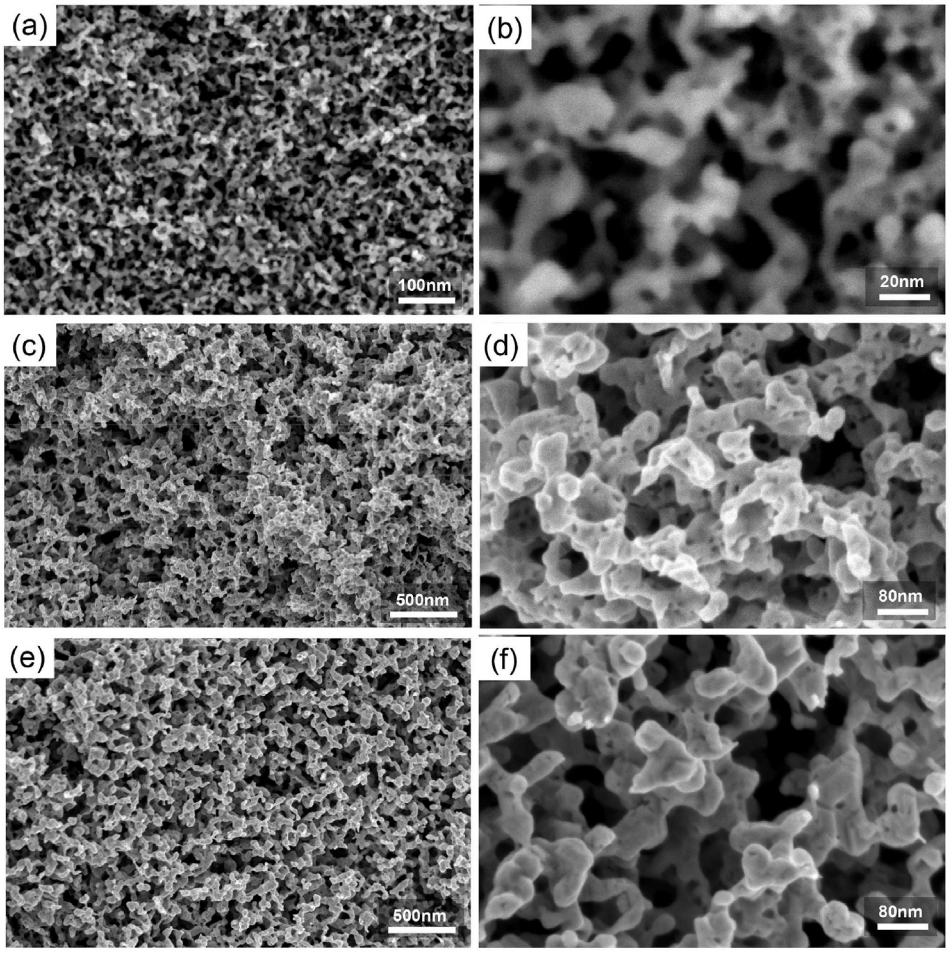

Fig. 4. Morphology of np Pd from electrochemical dealloying of a $Cu_{85}Pd_{15}$ master alloy in 1M H_2SO_4 at different temperature: (a–b) 25 °C, (c–d) 60 °C, and (e–f) 80 °C.

pore size distribution connects to the fraction, x^0_{Pd}, of Pd in the master alloy. Only a small composition window is accessible, since nanoporous bodies made from Cu-Pd master alloys with $x^0_{Pd} < 0.15$ are fragile, and since master alloys with $x^0_{Pd} \geq 0.25$ could not be completely dealloyed. Two master alloys of our study fall within that window, namely with $x^0_{Pd} = 0.15$ (see previous Sections) and $x^0_{Pd} = 0.20$. The last-mentioned material was dealloyed in 1M H_2SO_4 at 60 °C with an applied potential of 0.835 V, followed by electrochemical reduction. EDX measurements indicate 5.0 ± 1.5 at % residual Cu.

Fig. 5 compares scanning electron micrographs on cleavage surfaces of np Pd from the two master alloys. At the upper hierarchy level, both porous structures consistently display the rather open metal network, with slender ligaments separated by much larger (Type II) pores. The master alloy with the higher Pd fraction yields a somewhat denser structure (Fig. 5b). This is consistent with the expectation that the phase fraction reflects the initial Pd fraction. Both materials display a bimodal pore structure. Yet, the amount of lower-level (Type I) porosity is noticeably less in the material made from the master alloy with higher Pd fraction.

3.5. Structure evolution during primary and secondary corrosion

Why are there two structural length scales in our as-prepared np Pd? For clarifying the evolution of the structure during the corrosion we carried out an incomplete dealloying. We used 1M H_2SO_4 at 60 °C and dealloying potential at 790 mV. The dealloying was stopped when the charge transfer reached about two thirds of what Faraday's law requires for dissolving all Cu. The sample was then cleaved and the resulting cross-section surface, which intersects the sample center, was investigated by SEM and EDX characterization, see Fig. 6. The image series affords an inspection of the structure evolution. The innermost region of the image (point P1 in the overview of Fig. 6a) represents the structure near the dealloying front, in other words, the nanoporous metal shortly after primary dealloying. Image regions closer to the external surface of the sample (points P2-P4) present porous metal that has been exposed to the corrosion for successively longer time. These regions have undergone a substantial amount of secondary dealloying, that is, a combination of coarsening and further corrosion. Therefore, inspection of the structures and the various points provides insight into the evolution of the pore structure and composition with time during primary and secondary corrosion.

With reference to the point closest to the surface, P4, we note that structure as well as residual copper fraction—to be discussed below—are comparable to a completely dealloyed sample, see Fig. 4c–d. Therefore, the sequence of structures in Fig. 6 is representative of the structural evolution during our preparation protocol.

Fig. 6b shows the pore structure in the sample center. It is seen that the entire sample is porous, even though only two thirds of the Cu has been removed. This is consistent with a residual copper fraction of 50 at.-% in this region. Such high retention of the less noble element of the primary dealloying is in fact well compatible

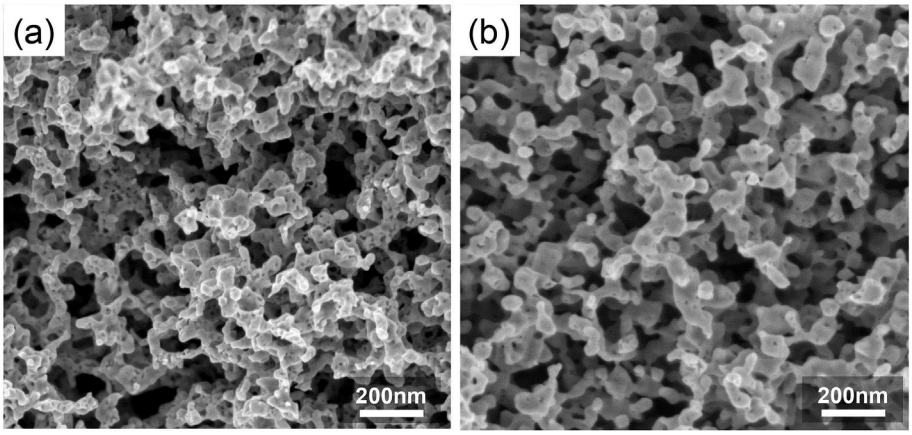

Fig. 5. Morphology of np Pd from electrochemical dealloying of master alloys: (a) $Cu_{85}Pd_{15}$ and (b) $Cu_{80}Pd_{20}$ in 1M H_2SO_4 at 60°C.

with what is known about dealloying, see for instance the study of Ag-Au dealloying in Ref. [55]. Inspection of the residual copper fractions at points P2-P4 (Fig. 6b–h), which were exposed to corrosion for successfully longer times, shows the removal of copper during secondary dealloying, with the residual copper fraction in the surface-near regions (P4) down to 8 at.%.

Fig. 6b shows two distinct types of pores, and the distinction in fact can be carried through the entire image sequence of Fig. 6. Type I pores are smaller and appear roughly cylindrical, whereas Type II pores are larger and have an elongated, crack-like shape. Furthermore, the diameter of the Type I pores at P1 is close to the diameter of solid struts (ligaments). By contrast, the Type II pores are several times larger than diameter of the struts. Secondary corrosion in the image sequence from P2 to P4 leaves the size of the Type I pores constant. These pores are embedded in solid regions that thicken during secondary corrosion. The interjacent Type II pores also increase in size. At the same time, the images show the pore volume fraction increases. At P4, where the longest secondary dealloying was experienced, the micrographs reveal a well-defined hierarchical nanoporous structure (Fig. 6g–h).

3.6. Coarsening of hierarchical np Pd by annealing

The hierarchical np Pd samples obtained from $Cu_{85}Pd_{15}$ master alloy at a dealloying temperature of 60°C were taken as starting material for a series of thermal treatments in vacuum. The resulting morphologies for the fracture surfaces of samples obtained with different annealing temperatures are presented in Fig. 7. It was observed that a five-minute annealing treatment at temperatures between 200°C and 400°C replaces the structural hierarchy with a unimodal pore structure. The final ligament sizes of the annealed samples increased from several tens of nanometers to hundreds of nanometers with increasing annealing temperature. By randomly measuring the diameter of 20 ligaments for each sample and taking at least two samples for each annealing condition, the average ligament sizes of the annealed samples were estimated to be 80 nm at 200°C, 120 nm at 300°C, and 270 nm at 400°C.

4. Discussion

In this work, several dealloying parameters including concentration of electrolytes, composition of master alloy, dealloying temperature and potential were explored via the potentiodynamic polarization approach, in-situ dilatometry, and morphology characterization via SEM. Dealloying of mm-sized $Cu_{85}Pd_{15}$ master alloy in 1M H_2SO_4 at 25–80°C produced uniform hierarchical np Pd in all investigated cases.

In view of the well-documented formation of a unimodal nanoscale network structure with pores and struts of similar size in Ag-Au dealloying, the formation of a multiscale pore structure in our experiment is remarkable. Such multiscale structures are frequently observed when dealloying multiphase master alloys. The pore structure then reflects the microstructure that was created during solidification of the master alloy. However, $Cu_{85}Pd_{15}$ is single phase at equilibrium at all temperatures [45]. Solidus and liquidus are so close as to make the solidification near 1100°C quasi polymorphic, and the ordering transformation—if it were to occur during the rapid cooling of our master alloy—to an off-stoichiometric $L1_2$ structure [45] would also be polymorphic. The hierarchical structure is therefore not preformed but must be generated during the corrosion.

Morphologies similar to the present one have been observed after single step dealloying of Cu_3Au [56,57]. The observation was linked to the addition of potassium iodide [56] or of inhibiting thiol molecules [57] to the 0.1M H_2SO_4 base electrolyte. The resulting passivation layer leads to pitting-like processes and to an instable corrosion front that generates structure on different length scales in thin layers near the external surface. It appears obvious that this mechanism does not apply to the present situation: Copper oxide or -sulfide species are soluble and so the trend for passivation is expected weak. Single-step dealloying of the ternary metallic glass $Pd_{30}Ni_{50}P_{20}$ in sulfuric acid was also observed to form hierarchical nanoporous structure in palladium. The different dissolution rates between P and Ni [42] were invoked for rationalizing the observation. The mechanism cannot be transferred to our dealloying of a binary master alloy.

It is significant that the multiscale pore structure emerges already at the onset of corrosion, that is, after primary dealloying (compare Fig. 6b). Compositional heterogeneity in the master alloy would be an obvious explanation. The larger Type II pores would then represent Cu-rich regions of the solid solution, which would be dissolved preferentially. The presence of paths of preferential dissolution would be reminiscent of the percolating cluster concept as proposed by Sieradzki et al. [1]. The existence of such regions at the scale of Type II pore size, namely tens of nm, would presuppose an incipient (spinodal?) demixing in the master alloy. Yet, as argued above, the alloy phase diagram provides no support for demixing. In the contrary, the presence of ordering at low temperature testifies to a negative enthalpy of mixing. These considerations lead us to qualify the scenario of preformed copper-rich regions as unlikely.

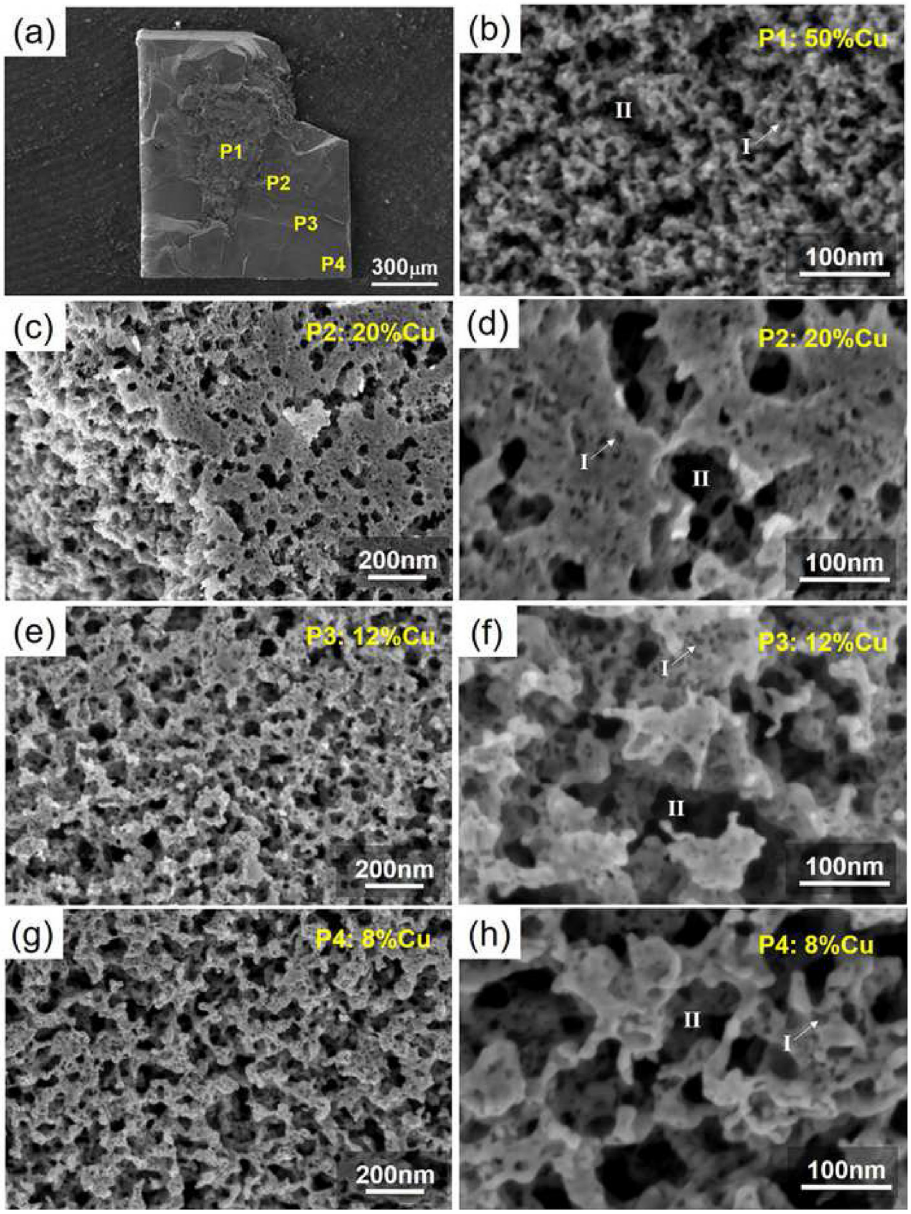

Fig. 6. Cross-sectional analysis of partially-dealloyed samples: (a) SEM image of a fracture surface of a partially dealloyed sample by electrochemical dealloying a $Cu_{85}Pd_{15}$ master alloy in 1M H_2SO_4 at 60°C, (b–h) high-resolution SEM images of the four representative positions P1-P4 as indicated in (a). The local residual Cu concentration is also indicated for the different positions. For classification of type I and type II pores, see text.

A more likely scenario may be linked to the unusually low fraction of the more noble element, Pd, in our alloy. Since there is negligible shrinkage during dealloying, the solid volume fraction, φ, of the final porous material will sensibly coincide with the Pd fraction in the master alloy. As stated in the results section, we indeed measured $\varphi \sim 17\%$ for samples based on $Cu_{85}Pd_{15}$ master alloy. Soyarslan et al. [58] have recently pointed out that random-field, spinodal-like structures achieve an excellent agreement with the φ-dependent elastic properties of dealloying-made nanoporous gold. Significantly, these structures undergo a percolation-to-cluster transition and become disconnected when their solid fraction falls below $\varphi = 16\%$. It is therefore remarkable that SEM's of the present material display a well-connected structure in spite of the low φ. Apparently, the microstructure evolution is not readily explained in terms of the conventional combination of less-noble element dissolution and curvature-driven coarsening. In fact, the observation that the conventional mechanism involves a progressive loss of connectivity as the dissolution advances suggests a loss of local mechanical stability during primary corrosion. This loss may be particularly severe for our material with its low more-noble element fraction. We hypothesize that, at an intermediate stage of the dissolution process, the loss of stability results in a local densification by rigid body displacement and agglomeration of neighboring, loosely connected parts of the network. The agglomeration will form coarser ligaments surrounded by even larger pores. At the level of the Type II pores, the crack-like morphology shown in Fig. 6 is indeed compatible with the notion of a disproportionation into densified regions separated by large pores. Furthermore, the sequence of structures between image parts P1 and P4 in that figure is compatible with a further collapse

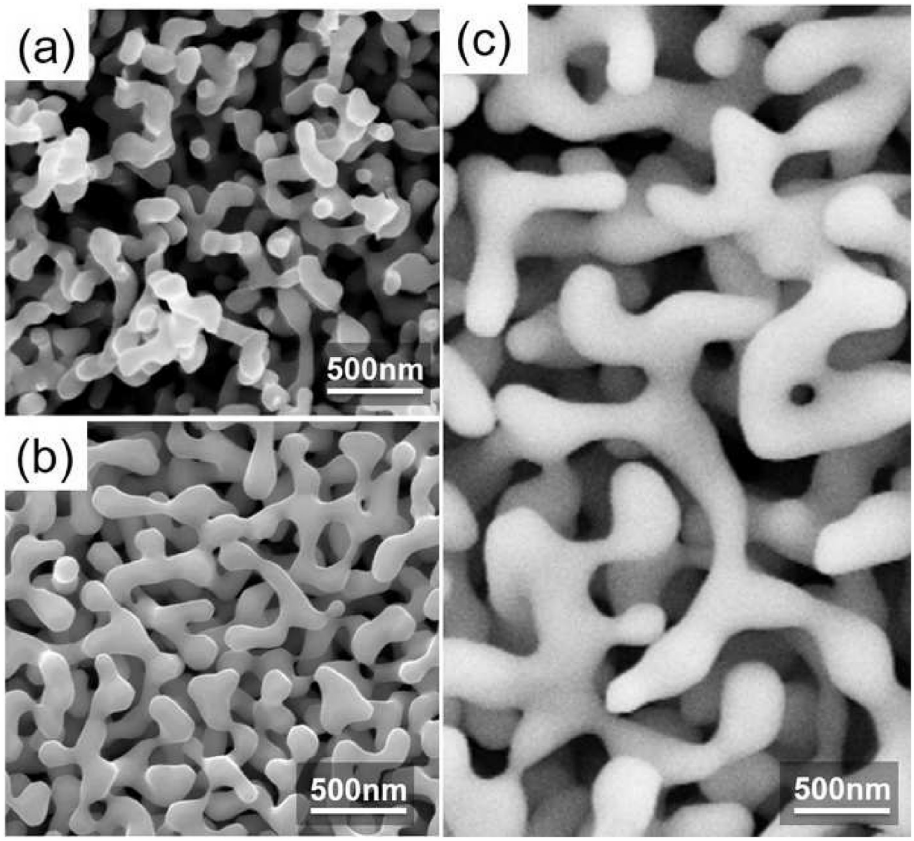

Fig. 7. SEM images of a fracture surface of np Pd samples based on $Cu_{85}Pd_{15}$ master alloy annealed for 5 min at different temperatures: (a) 200°C, (c) 300°C, (d) 400°C.

of the structure, opening up the larger Type II pores while the solid parts densify further. The agglomerated ligaments contain residual copper and can form small-scale porosity upon further dissolution. The schematics of Fig. 8 illustrates the successive stages of that process. Overall, the experimental observations and the above considerations on mechanisms favor local structure collapse due to low solid fraction as the mechanism behind the bimodal pore size distribution.

It is remarkable that annealing replaces the bimodal pore structure with a classic nanoporous network structure with a single characteristic length scale. This observation may be understood as the consequence of the largely different timescales for microstructure evolution at the two regimes of pore size. A simple analysis of curvature-driven and surface-diffusion mediated coarsening suggests a growth law with a time exponent $n = \frac{1}{4}$ [59]. Experiment on coarsening of dealloying-made nanoporous metal does not unanimously support that expectation (see specifically Ref. [60]), yet most data agrees with coarsening drastically slowing down as the ligament size increases [61,62]. This implies that the smaller Type I pores coarsen much faster than the larger Type II ones. Furthermore, atomistic studies [63] confirm that the outer surface of a small porous body acts as a sink for free volume, promoting densification during coarsening. This situation applies to the coarsening of the Type I pores, since they are confined in the nanoscale ligaments of the upper hierarchy level. In other words, it is natural to assume that coarsening of the bimodal pore structure

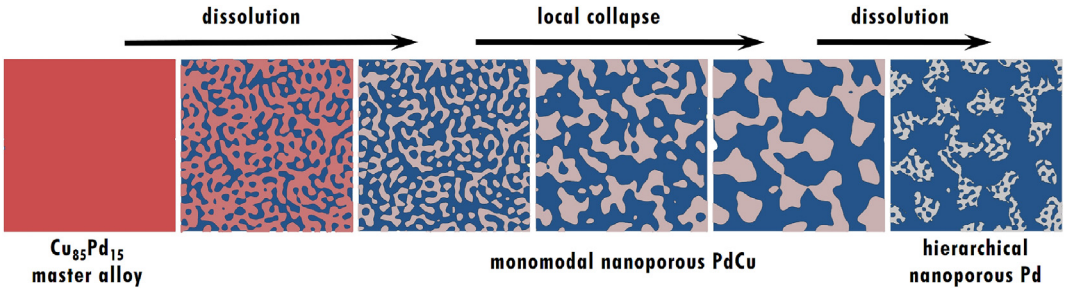

Fig. 8. Suggested scheme for the formation of the hierarchical pore structure during corrosion of a Cu-rich (symbolized by reddish color) Cu-Pd solid solution. Initial stages of dissolution reduce the connectivity between the solid ligaments, enabling the disproportionation into coarse and dense ligaments and large pores (blue) by rigid body displacement and agglomeration of the loosely connected solid regions. Ongoing dissolution then further reduces the solid fraction in larger ligaments of Pd (grayish color) at the upper hierarchy level and results in the formation of small pores at the lower hierarchy level. (For interpretation of the references to color in this figure legend, the reader is referred to the Web version of this article.)

removes the Type I porosity by transporting its free volume to the outer surface of the ligaments of the upper hierarchy level. This notion is in good agreement with the observation that coarsening establishes a unimodal pore structure.

5. Conclusions

In this work, a systematic development of an optimal electrochemical synthesis route in order to produce np Pd was done. In the beginning, we determined the preferable chemical composition of the master alloy as $Cu_{85}Pd_{15}$ and the optimal concentration of electrolyte as 1M sulfuric acid via investigating the corrosion behavior via potentiodynamic polarization experiments. Following that, the impact of electrode potential on the samples' dimension changes and the impact of dealloying temperature on the samples' morphologies after electrochemical treatment were explored.

Consistent with our previous work [11], dealloying of $Cu_{85}Pd_{15}$ alloy in 1M sulfuric acid at an elevated temperature was a facile strategy to produce uniform, hierarchical nanoporous np Pd without cracks as bulk samples. The open question why did a one step template-free dealloying single phase binary alloys like $Cu_{85}Pd_{15}$ yield uniform well-defined hierarchical np structure instead of a typical unimodal porous structure was discussed, and structural instability due to the low content in more noble element was suggested as the underlying mechanism.

Finally, this work establishes np Pd with self-similar classic unimodal porous structure with tunable ligament size (80–270 nm) by simply annealing hierarchical np Pd, as a second model system following np gold for studying the mechanical behavior of nanostructured metals via conventional testing strategies.

Acknowledgements

Shan Shi acknowledges support by the Chinese Scholarship Council. Support by the German Research Foundation within SFB 986 "Tailor-Made Multi-Scale Materials Systems - M^3", projects B2 and B8, is also acknowledged.

Appendix A

A1. Local coarsening induced by the electron beam of the SEM

As shown in the preceding paragraph, we can convert the hierarchical np structure into a unimodal pore structure via a simple post-annealing procedure under high vacuum atmosphere (Fig. 7). It was even possible to do an in-situ analysis on structure evolution during the coarsening process of hierarchical np Pd by using the local heat produced by the electron beam of the SEM itself. In Fig. A1, the disappearance of the lower level type-I pores and neck growth of ligaments can be clearly seen.

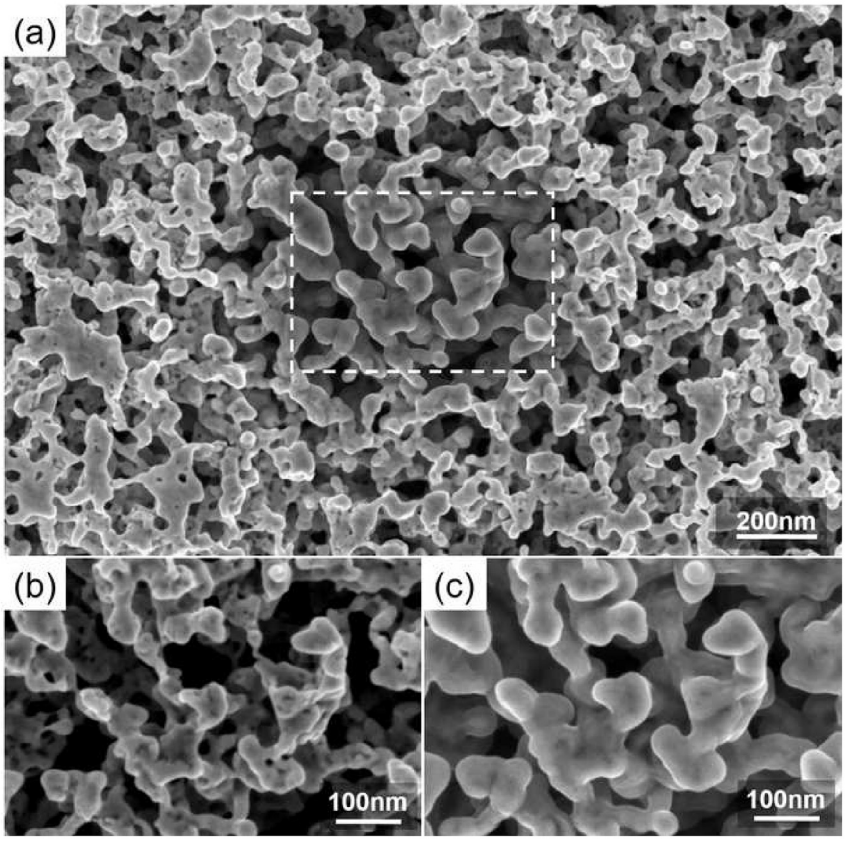

Fig. A1. SEM images of locally annealed hierarchical nanoporous palladium by the electron beam in a SEM. (a) Overview of np Pd after after local heating. The treated area is marked by a dashed rectangle. Also shown are images at higher resolution of the marked area (b) before and (c) after heating.

References

[1] K. Sieradzki, R. Corderman, K. Shukla, R. Newman, Computer simulations of corrosion: selective dissolution of binary alloys, Philos. Mag. A 59 (4) (1989) 713–746.
[2] J. Erlebacher, M.J. Aziz, A. Karma, N. Dimitrov, K. Sieradzki, Evolution of nanoporosity in dealloying, Nature 410 (6827) (2001) 450–453.
[3] J. Weissmüller, K. Sieradzki, Dealloyed nanoporous materials with interface-controlled behavior, MRS Bull. 43 (1) (2018) 14–19.

[4] V. Zielasek, B. Jürgens, C. Schulz, J. Biener, M.M. Biener, A.V. Hamza, M. Bäumer, Gold catalysts: nanoporous gold foams, Angew. Chem. Int. Ed. 45 (48) (2006) 8241–8244.
[5] C. Xu, J. Su, X. Xu, P. Liu, H. Zhao, F. Tian, Y. Ding, Low temperature CO oxidation over unsupported nanoporous gold, J. Am. Chem. Soc. 129 (1) (2007) 42–43.
[6] Y. Ding, M. Chen, Nanoporous metals for catalytic and optical applications, MRS Bull. 34 (8) (2009) 569–576.
[7] D. Kramer, R.N. Viswanath, J. Weissmüller, Surface-stress induced macroscopic bending of nanoporous gold cantilevers, Nano Lett. 4 (5) (2004) 793–796.
[8] H.-J. Jin, X.-L. Wang, S. Parida, K. Wang, M. Seo, J. Weissmuller, Nanoporous Au-Pt alloys as large strain electrochemical actuators, Nano Lett. 10 (1) (2009a) 187–194.
[9] E. Detsi, S. Punzhin, J. Rao, P.R. Onck, J.T.M. De Hosson, Enhanced strain in functional nanoporous gold with a dual microscopic length scale structure, ACS Nano 6 (5) (2012) 3734–3744.
[10] J. Zhang, Q. Bai, Z. Zhang, Dealloying-driven nanoporous palladium with superior electrochemical actuation performance, Nanoscale 8 (13) (2016) 7287–7295.
[11] S. Shi, J. Markmann, J. Weissmüller, Actuation by hydrogen electrosorption in hierarchical nanoporous palladium, Phil. Mag. 97 (19) (2017) 1571–1587.
[12] C. Cheng, L. Luhrs, T. Krekeler, M. Ritter, J. Weissmuller, Semiordered hierarchical metallic network for fast and large charge-induced strain, Nano Lett. 17 (8) (2017) 4774–4780.
[13] S. Kucheyev, J. Hayes, J. Biener, T. Huser, C. Talley, A. Hamza, Surface-enhanced Raman scattering on nanoporous Au, Appl. Phys. Lett. 89 (5) (2006), 053102.
[14] L. Qian, X. Yan, T. Fujita, A. Inoue, M. Chen, Surface enhanced Raman scattering of nanoporous gold: smaller pore sizes stronger enhancements, Appl. Phys. Lett. 90 (15) (2007), 153120.
[15] H. Liu, L. Zhang, X. Lang, Y. Yamaguchi, H. Iwasaki, Y. Inouye, Q. Xue, M. Chen, Single molecule detection from a large-scale SERS-active $Au^{79}Ag^{21}$ substrate, Sci. Rep. 1 (2011) 112.
[16] X. Li, B. Huang, C. Qiu, Z. Li, L.-H. Shao, H. Liu, Hierarchical nested-network porous copper fabricated by one-step dealloying for glucose sensing, J. Alloys Compd. 681 (2016) 109–114.
[17] C. Stenner, L.-H. Shao, N. Mameka, J. Weissmüller, Piezoelectric gold: strong charge-load response in a metal-based hybrid nanomaterial, Adv. Funct. Mater. 26 (28) (2016) 5174–5181.
[18] E. Şeker, W.-C. Shih, K.J. Stine, Nanoporous metals by alloy corrosion: bioanalytical and biomedical applications, MRS Bull. 43 (1) (2018) 49–56.
[19] Q. Chen, Y. Ding, M. Chen, Nanoporous metal by dealloying for electrochemical energy conversion and storage, MRS Bull. 43 (1) (2018) 43–48.
[20] J. Biener, A.M. Hodge, A.V. Hamza, L.M. Hsiung, J.H. Satcher Jr., Nanoporous Au: a high yield strength material, J. Appl. Phys. 97 (2) (2005), 024301.
[21] C. Volkert, E. Lilleodden, D. Kramer, J. Weissmüller, Approaching the theoretical strength in nanoporous Au, Appl. Phys. Lett. 89 (6) (2006), 061920.
[22] R. Li, K. Sieradzki, Ductile-brittle transition in random porous Au, Phys. Rev. Lett. 68 (8) (1992) 1168.
[23] N. Senior, R. Newman, Synthesis of tough nanoporous metals by controlled electrolytic dealloying, Nanotechnology 17 (9) (2006) 2311–2316.
[24] H.-J. Jin, L. Kurmanaeva, J. Schmauch, H. Rösner, Y. Ivanisenko, J. Weissmüller, Deforming nanoporous metal: role of lattice coherency, Acta Mater. 57 (9) (2009b) 2665–2672.
[25] N.J. Briot, T. Kennerknecht, C. Eberl, T.J. Balk, Mechanical properties of bulk single crystalline nanoporous gold investigated by millimetre-scale tension and compression testing, Phil. Mag. 94 (8) (2014) 847–866.
[26] L.-Z. Liu, X.-L. Ye, H.-J. Jin, Interpreting anomalous low-strength and low-stiffness of nanoporous gold: quantification of network connectivity, Acta Mater. 118 (2016) 77–87.
[27] N. Mameka, K. Wang, J. Markmann, E.T. Lilleodden, J. Weissmüller, Nanoporous goldtesting macro-scale samples to probe small-scale mechanical behavior, Mater. Res. Lett. 4 (1) (2016) 27–36.
[28] N. Badwe, X. Chen, K. Sieradzki, Mechanical properties of nanoporous gold in tension, Acta Mater. 129 (2017) 251–258.
[29] H.-J. Jin, J. Weissmüller, A material with electrically tunable strength and flow stress, Science 332 (6034) (2011) 1179–1182.
[30] S. Sun, X. Chen, N. Badwe, K. Sieradzki, Potential-dependent dynamic fracture of nanoporous gold, Nat. Mater. 14 (9) (2015) 894–898.
[31] N. Mameka, J. Markmann, J. Weissmüller, On the impact of capillarity for strength at the nanoscale, Nat. Commun. 8 (1) (2017) 1976.
[32] L. Luhrs, B. Zandersons, N. Huber, J. Weissmuller, Plastic Poissons ratio of nanoporous metals: a macroscopic signature of tension–compression asymmetry at the nanoscale, Nano Lett. 17 (10) (2017) 6258–6266.
[33] H.-J. Jin, J. Weissmüller, D. Farkas, Mechanical response of nanoporous metals: a story of size, surface stress, and severed struts, MRS Bull. 43 (1) (2018) 35–42.
[34] T. Wada, H. Kato, Three-dimensional open-cell macroporous iron, chromium and ferritic stainless steel, Scripta Mater. 68 (9) (2013) 723–726.
[35] J.W. Kim, M. Tsuda, T. Wada, K. Yubuta, S.G. Kim, H. Kato, Optimizing niobium dealloying with metallic melt to fabricate porous structure for electrolytic capacitors, Acta Mater. 84 (2015) 497–505.
[36] I. McCue, A. Karma, J. Erlebacher, Pattern formation during electrochemical and liquid metal dealloying, MRS Bull. 43 (1) (2018a) 27–34.
[37] I. Okulov, A. Okulov, I. Soldatov, B. Luthringer, R. Willumeit-Römer, T. Wada, H. Kato, J. Weissmüller, J. Markmann, Open porous dealloying-based biomaterials as a novel biomaterial platform, Mater. Sci. Eng. C 88 (2018) 95–103.
[38] J. Yu, Y. Ding, C. Xu, A. Inoue, T. Sakurai, M. Chen, Nanoporous metals by dealloying multicomponent metallic glasses, Chem. Mater. 20 (14) (2008) 4548–4550.
[39] Z. Qi, J. Weissmüller, Hierarchical nested-network nanostructure by dealloying, ACS Nano 7 (7) (2013) 5948–5954.
[40] H. Duan, Q. Hao, C. Xu, Hierarchical nanoporous PtTi alloy as highly active and durable electrocatalyst toward oxygen reduction reaction, J. Power Sources 280 (2015) 483–490.
[41] T. Juarez, J. Biener, J. Weissmüller, A.M. Hodge, Nanoporous metals with structural hierarchy: a review, Adv. Eng. Mater. 19 (2017), 1700389.
[42] Y. Ding, J. Erlebacher, Nanoporous metals with controlled multimodal pore size distribution, J. Am. Chem. Soc. 125 (26) (2003) 7772–7773.
[43] H.-J. Qiu, Y. Ito, M. Chen, Hierarchical nanoporous nickel alloy as three-dimensional electrodes for high-efficiency energy storage, Scripta Mater. 89 (2014) 69–72.
[44] Q. Kong, L. Lian, Y. Liu, J. Zhang, L. Wang, W. Feng, Bulk hierarchical nanoporous palladium prepared by dealloying PdAl alloys and its electrochemical properties, Microporous Mesoporous Mater. 208 (2015) 152–159.
[45] T.B. Massalski, H. Okamoto, P.R. Subramanian, L. Kacprzak, Binary Alloy Phase Diagrams, ASM International, Materials Park, OH, 1990.
[46] J. Weissmüller, R.C. Newman, H.-J. Jin, A.M. Hodge, J.W. Kysar, Nanoporous metals by alloy corrosion: formation and mechanical properties, MRS Bull. 34 (8) (2009) 577–586.
[47] Q. Xu, Nanoporous Materials: Synthesis and Applications, CRC Press, 2013.
[48] K. Sieradzki, N. Dimitrov, D. Movrin, C. McCall, N. Vasiljevic, J. Erlebacher, The dealloying critical potential, J. Electrochem. Soc. 149 (8) (2002) B370–B377.
[49] K. Sieradzki, Curvature effects in alloy dissolution, J. Electrochem. Soc. 140 (10) (1993) 2868–2872.
[50] S. Parida, D. Kramer, C. Volkert, H. Rösner, J. Erlebacher, J. Weissmüller, Volume change during the formation of nanoporous gold by dealloying, Phys. Rev. Lett. 97 (3) (2006), 035504.
[51] Y. Zhong, J. Markmann, H.-J. Jin, Y. Ivanisenko, L. Kurmanaeva, J. Weissmüller, Crack mitigation during dealloying of $Au^{25}Cu^{75}$, Adv. Eng. Mater. 16 (4) (2014) 389–398.
[52] E. Detsi, M. Van De Schootbrugge, S. Punzhin, P. Onck, J. De Hosson, On tuning the morphology of nanoporous gold, Scripta Mater. 64 (4) (2011) 319–322.
[53] A. Dursun, D. Pugh, S. Corcoran, Dealloying of Ag-Au alloys in halide-containing electrolytes affect on critical potential and pore size, J. Electrochem. Soc. 150 (7) (2003) B355–B360.
[54] L. Qian, M. Chen, Ultrafine nanoporous gold by low-temperature dealloying and kinetics of nanopore formation, Appl. Phys. Lett. 91 (8) (2007), 083105.
[55] T. Krekeler, A.V. Strasser, M. Graf, K. Wang, C. Hartig, M. Ritter, J. Weissmüller, Silver-rich clusters in nanoporous gold, Mater. Res. Lett. 5 (5) (2017) 314–321.
[56] G.N. Ankah, A. Pareek, S. Cherevko, A.A. Topalov, M. Rohwerder, F.U. Renner, The influence of halides on the initial selective dissolution of Cu^3 Au (111), Electrochim. Acta 85 (2012) 384–392.
[57] G.N. Ankah, A. Pareek, S. Cherevko, J. Zegenhagen, F.U. Renner, Hierarchical nanoporous films obtained by surface cracking on Cu-Au and ethanethiol on Au (001), Electrochim. Acta 140 (2014) 352–358.
[58] C. Soyarslan, S. Bargmann, M. Pradas, J. Weissmüller, 3D stochastic bicontinuous microstructures: generation, topology and elasticity, Acta Mater. 149 (2018) 326–340.
[59] C. Herring, Effect of change of scale on sintering phenomena, J. Appl. Phys. 21 (4) (1950) 301–303.
[60] Y.-c. K. Chen-Wiegart, S. Wang, Y.S. Chu, W. Liu, I. McNulty, P.W. Voorhees, D.C. Dunand, Structural evolution of nanoporous gold during thermal coarsening, Acta Mater. 60 (12) (2012) 4972–4981.
[61] S. Kuwano-Nakatani, T. Fujita, K. Uchisawa, D. Umetsu, Y. Kase, Y. Kowata, K. Chiba, T. Tokunaga, S. Arai, Y. Yamamoto, N. Tanaka, M.W. Chen, Environment-sensitive thermal coarsening of nanoporous gold, Mater. Trans. 56 (4) (2015) 468–472.
[62] I. McCue, J. Stuckner, M. Murayama, M.J. Demkowicz, Gaining new insights into nanoporous gold by mining and analysis of published images, Sci. Rep. 8 (2018b) 6761.
[63] J. Erlebacher, Mechanism of coarsening and bubble formation in high-genus nanoporous metals, Phys. Rev. Lett. 106 (22) (2011), 225504.